Real-Time Monitoring of Competing Nanoparticle Formation Pathways during Cation Exchange Using Benchtop Light Scattering

Gabriella A. Di Domizio,¹ Lucas T. Alameda,¹ Julian Fanghanel,² Robert W. Lord,¹ Jennifer R. Miller,¹ and Raymond E. Schaak^{1,3,4,*}

Abstract

Cation exchange is an increasingly common pathway for nanoparticle synthesis, as it modifies the composition in a controllable way while maintaining other key features, including crystal structure and morphology. However, cation exchange pathways can compete with other nanoparticle formation pathways, depending on the system and reaction conditions. Simple strategies for monitoring such reactions can therefore be informative. Here, we use benchtop light scattering with a laser pointer as a simple tool to monitor putative cation exchange reactions and to help differentiate, in real time, between pathways that involve cation exchange vs pathways that involve dissolution and re-precipitation. We use the transformation of digenite copper sulfide into manganese sulfide as a model system. When a laser pointer shines through the reaction flask as digenite copper sulfide nanoparticles react with Mn²⁺ at 100 °C. light scattering is observed continuously, indicating that nanoparticles are present during the entire reaction as would be required for a cation exchange pathway. At higher temperatures, light scattering disappears and then re-appears, indicating that nanoparticles are not always present and that a different pathway involving dissolution and re-precipitation is operable. Using this approach, along with additional control experiments, we were able to identify the threshold temperature below which zincblende MnS, a metastable polymorph, forms through a cation exchange pathway. We were also able to establish that at higher temperatures the thermodynamically favored product, rocksalt MnS, forms through a dissolution-reprecipitation pathway. These results provide useful insights into the temperature dependence of a model cation exchange reaction and suggest that light scattering could provide high-level insights, in real time on the benchtop, into nanoparticle reaction pathways that involve post-synthetic modifications where multiple competing pathways could be possible.

¹ Department of Chemistry, ² Department of Materials Science and Engineering, ³ Department of Chemical Engineering, and ⁴ Materials Research Institute, The Pennsylvania State University, University Park, PA 16802

Introduction

Nanocrystal cation exchange offers a powerful low-temperature solution-based strategy for synthesizing solid-state compounds having crystal structures that are metastable in bulk and therefore inaccessible using thermally-driven methods. ^{1–9} Using this approach, cations dissolved in solution can replace cations in a nanocrystal. Such exchange reactions generally require nanocrystals having highly mobile cations, as well as a chemical driving force that makes it favorable to expel the cations into solution. These characteristics result in cation exchange reactions that occur very rapidly, *i.e.* on the time scale of seconds to minutes, and at relatively low temperatures, *i.e.* room temperature through ~100 °C. The anion sublattice is comparatively rigid, which means that at these temperatures, the structure does not significantly change as cations are shuttled in and out. As a result, the overall crystal structure can be retained during cation exchange reactions, and these structure-templating effects can result in the formation of crystal structures that are not observed in bulk systems made through higher-temperature methods. As just a few examples, zincblende and wurtzite CdSe transform to zincblende and wurtzite ZnSe, respectively, ⁵ and zincblende and wurtzite MnS, CoS, ZnS, CdS, and CuInS₂ form from structurally-related digenite and roxbyite Cu_{1.8}S, respectively. ^{7,8}

The MnS system is particularly interesting from the perspective of crystal structure. For MnS, rocksalt is the most stable crystal structure and therefore the one that forms upon combining the elements at high temperatures or through direct precipitation methods. ^{10,11} However, the wurtzite polymorph of MnS can be synthesized by exchanging the Cu⁺ cations in roxbyite Cu_{1.8}S with Mn²⁺. Roxbyite has a distorted hexagonal close packed (hcp) sulfur sublattice that is retained in wurtzite MnS, which also has hcp sulfur anions. The zincblende polymorph of MnS can also be synthesized by applying an analogous Mn²⁺ cation exchange reaction to digenite Cu_{1.8}S, which has the same cubic close packed (ccp) sulfur sublattice as the zincblende structure. Pathways therefore exist to synthesize three distinct polymorphs of MnS: rocksalt by direct solvothermal precipitation, wurtzite by Mn²⁺ exchange of roxbyite, and zincblende by Mn²⁺ exchange of digenite.

To be successful, cation exchange reactions must be run under conditions where the only reaction happening is cation exchange. There must be sufficient thermal energy to facilitate cation diffusion, which is a prerequisite to exchange. However, if the reaction temperature is too high, there could be sufficient thermal energy for the sublattice structure to rearrange, transforming a targeted metastable phase into a more stable product. This could, in principle, occur in two ways – concomitant with cation exchange, where higher temperatures cause the anion sublattice to rearrange as cation diffusion is happening, or a thermally-induced phase transition after cation exchange is complete. At the same time, there could be a competition between reaction pathways at elevated temperatures, such as a threshold temperature below which cation exchange occurs and above which dissolution and reprecipitation occurs. Surveying the systems that have been accessed using nanocrystal cation exchange, many products retain the structural features of the precursor, but many do not.^{2,12–14} It is important to identify the pathway by which a precursor transforms to a product during a putative cation exchange reaction, *i.e.* whether or not the reaction indeed proceeds through a cation exchange process, especially if the product does not retain the structure of the precursor.

Probing reaction pathways *in situ* can be challenging, as it requires methods capable of examining transient species that are present while the reaction is happening. Various spectroscopic and diffraction techniques have uncovered important details of reaction pathways and intermediates, ^{15–17} but they typically require high flux methods, specialized or custom-built reactors, and/or fast time scales that can only be carried out at a limited number of facilities

worldwide and require significant time and analytical rigor. *In situ* microscopy methods offer powerful glimpses into nanocrystal formation reactions, ^{18,19} but are limited in scope because of constraints on temperature and chemical reactivity that can be accommodated by sample holders. For nanoparticle cation exchange, the most common method for probing reactions is the extraction and analysis of aliquots to identify the isolatable species that are present at various time points throughout the reaction. ²⁰ While useful, this approach can not differentiate some of the alternative and competing reaction pathways that may be occurring during the course of the reaction, such as dissolution and reprecipitation. Comparison of particle size, shape, and uniformity before and after cation exchange reactions can also be used to support an exchange-based pathway, as they are expected to be nearly identical. However, even this approach does not explicitly rule out alternative pathways, such as dissolution and reprecipitation, as product nanoparticles may end up appearing similar in both cases. Additional methods include measuring changes in resistivity, ²¹ photoluminescence, ²² optical absorption, ^{4,23} scattering, ²⁴ and fluorescence, ⁴ which can be powerful, but are also limited to materials exhibiting appropriate properties that change throughout the cation exchange process.

Benchtop light scattering provides a potentially simple and inexpensive method for probing highlevel characteristics of reaction pathways relevant to cation exchange processes. Light scattering by particulate matter within its path is commonly used to determine if a colloidal dispersion is present. 25,26 The presence of colloidal particles in a solution can therefore be confirmed by observation of scattering; light, from a source such as a laser pointer, scatters and produces a visible light beam. It follows, then, that the absence of scattered light correlates with an absence of significant concentrations of colloidal particles in a solution. Benchtop light scattering therefore has the potential to differentiate a reaction pathway involving cation exchange, where colloidal particles remain present for the duration of a reaction, and an alternate dissolution/reprecipitation pathway, whereby the starting particles disappear in a separate step before the product particles form. Assuming that the timescales of dissolution and reprecipitation are slow enough to be observable macroscopically, which is reasonable for systems such as copper sulfide, 27,28 use of light scattering from a laser pointer could provide real-time insights into the likelihood of a cation exchange pathway, which would be useful mechanistically and also to help guide optimization of reaction conditions and subsequent mechanistic studies that are more in-depth and sophisticated.

Here, we study the temperature dependence of the cation exchange reaction of digenite copper sulfide, Cu_{1.8}S, with Mn²⁺ to produce MnS. We identify the threshold temperature necessary to facilitate cation exchange to produce zincblende MnS, which is the expected product that retains the cubic close packed anion sublattice of digenite. We also observe that at higher temperatures, the reaction forms rocksalt MnS, which is the thermodynamically favored product. We use light scattering from a laser pointer as a simple benchtop method to probe the nature of the reaction pathway. Despite both reactions occurring in the same cation exchange solution, benchtop light scattering, along with additional control experiments, allows us to confirm that rocksalt MnS forms through a dissolution-reprecipitation pathway, which is distinct from the cation exchange reaction that forms zincblende MnS. This provides useful insights into the temperature dependence of a model cation exchange reaction and suggests that benchtop light scattering could provide a powerful, yet simple, approach for uncovering high-level mechanistic insights, in real time, during synthesis.

Experimental Section

Chemicals and Materials. Manganese (II) chloride tetrahydrate [MnCl₂·4H₂O, ≥ 98%, ACS reagent grade] and sulfur powder [-325 mesh, 99.5%] were purchased from Alfa Aesar.

Copper(I) chloride [CuCl, 97% reagent grade], oleylamine [tg-OLAM, $C_{18}H_{37}N$, 70%, technical grade], 1-octadecene [ODE, $C_{18}H_{36}$, 90%, technical grade], and oleic acid [OA, $C_{18}H_{34}O_2$, 90%, technical grade] were purchased from Sigma-Aldrich. Tri-n-octylphosphine [TOP, $C_{24}H_{51}P$, 85%] was purchased from TCI America. All solvents used (isopropanol and hexanes) were of analytical grade. All chemicals were used and implemented as received without further purification.

Synthesis of Cubic Digenite Cu_{1.8}S Spheres. Digenite Cu_{1.8}S spheres were synthesized through modification of a previously published procedure.²⁹ In a 100 mL 3-neck round-bottom flask equipped with a reflux condenser, thermometer, rubber septum, and magnetic stir bar, 320 mg of sulfur powder (10 mmol) and 20 mL of ODE were added and placed under vacuum while stirring. The contents of the flask were heated at 120 °C for 1 h. While the flask heated, a second 50 mL 3-neck round-bottom flask was prepared (similarly equipped) where 990 mg of CuCl (10 mmol), 4 mL of OA, and 5 mL of OLAM were added. The 50 mL flask was then placed under vacuum while stirring and heating at 120 °C for 1 h. Once the degassing step was complete, both flasks were placed under an Ar blanket. The S-ODE solution (100 mL flask) was then heated to 200 °C while the CuCl solution (50 mL flask) was heated to 130 °C. Once both temperatures were reached (at the same time), a 10 mL syringe was used to transfer all of the hot CuCl solution into the S-ODE solution at 200 °C via a rapid injection. The mixture was allowed to react for 10 min. After the allotted time, the heating mantle was removed allowing the solution to cool to room temperature. Once cooled, the nanoparticles were then precipitated through a series of centrifugation steps. First, the nanoparticle solution was poured into two centrifugation tubes where isopropanol was added. After the first centrifugation, the supernatant liquid was decanted and the particles within the centrifuge tubes were dispersed in ~5 mL of hexanes along with an addition of isopropanol prior to another centrifugation. Additional precipitation/centrifugation steps with hexanes and isopropanol were repeated until the supernatant liquid appeared clear and colorless. Once completed, the nanoparticles were dispersed in hexanes in preparation for postsynthetic modification.

Cation Exchange of Digenite Cu_{1.8}S to form Zincblende MnS. Cation exchange with Mn²⁺ was performed using a modification of a previously published procedure. ^{6,7} In a 50 mL 3-neck roundbottom flask, equipped as described above with the addition of a thermocouple probe (instead of a thermometer), 140 mg of MnCl₂·4H₂O, 4 mL of OLAM, and 10 mL of ODE were added and placed under vacuum while stirring and heating at 120 °C for 1 h. Once the degassing step was complete, the reaction was placed under Ar flow and heated at 180 °C for 30 min to ensure the formation of a clear and colorless Mn²⁺ -oleylamine complex solution.²⁰ The solution was then transitioned from Ar flow to an Ar blanket as it cooled to 100 °C in preparation for cation exchange. In a separate septum-capped vial, 30 mg of as-prepared digenite Cu_{1.8}S nanoparticles were degassed and placed under an Ar blanket prior to addition of 3 mL of TOP. The TOP-digenite Cu_{1.8}S suspension was then sonicated for a few seconds followed by an additional vacuum/Ar step. Before the injection of the TOP-digenite Cu_{1.8}S suspension into the Mn²⁺-oleylamine complex solution at 100 °C, a red laser pointer (650 nm) was turned on and placed next to the 50 mL flask. Once appropriately positioned, the TOP-digenite Cu_{1.8}S suspension was swiftly injected at 100 °C and allowed to react for 10 min. From the point of injection up until 5 min was reached, the red laser pointer continuously shined through the round-bottom flask as photographs were taken with a Panasonic Lumix G7 camera in 4K burst mode. After 10 min, the reaction was cooled to room temperature by replacing the heating mantle with an ice-water bath. The nanoparticles were then precipitated by addition of cold isopropanol and centrifugation. After decanting the supernatant, the nanoparticles were then dispersed in ~5 mL of hexanes with the addition of isopropanol and centrifuged once more. The

precipitation/centrifugation steps with hexanes and isopropanol continued until the supernatant was clear and colorless. The final nanoparticle product was then dispersed in hexanes for further characterization.

Simultaneous formation of Zincblende and Rocksalt MnS from Digenite Cu_{1.8}S. This reaction was prepared identically to that as mentioned previously up to and including the step where the Mn²⁺-oleylamine complex solution was heated at 180 °C for 30 min under Ar flow. At this point, the reaction was transitioned to an Ar blanket and heated to 200 °C (instead of cooling down). Prior to reaching 200 °C, a TOP-digenite Cu_{1.8}S suspension was prepared (as mentioned previously) and proceeded to be swiftly injected into the solution at 200 °C once the red laser pointer was appropriately positioned next to the 50 mL round-bottom flask. Immediately following the TOP-digenite Cu_{1.8}S injection, photographs were taken with the Panasonic Lumix G7 camera in 4K burst mode as the laser pointer continuously shined through the flask up until 5 min was reached. After 10 min, the reaction was cooled to room temperature by replacing the heating mantle with an ice-water bath. The nanoparticle product was then precipitated, centrifuged, and stored following the procedure as outlined above.

Formation of Rocksalt MnS from the Dissolution of Digenite Cu_{1.8}S. This reaction was prepared identically to that as mentioned previously except instead of heating the Mn²⁺-oleylamine complex solution up to 200 °C under an Ar blanket, it was heated to 300 °C. Before approaching 300 °C, the TOP-digenite Cu_{1.8}S suspension was prepared (as outlined previously) for injection and the red laser pointer was positioned appropriately. The TOP-digenite Cu_{1.8}S suspension was then injected at 300 °C followed by photographs taken with the Panasonic Lumix G7 camera in 4K burst mode as the laser pointer continuously shined through the 50 mL round-bottom flask for 5 min. After 10 min, the reaction was air-cooled to 200 °C followed by an icewater bath to cool to room temperature. The nanoparticle product was then precipitated following the exact centrifugation steps as previously mentioned and stored in hexanes for further characterization.

Material Characterization. Powder X-ray diffraction (XRD) data were collected using a Bruker D-8 Advance X-ray Diffractometer with Cu K α radiation. Transmission electron microscopy (TEM) images were collected using a Tecnai G2 microscope operating at 200 kV. Dynamic Light Scattering (DLS) data were collected at 25 $^{\circ}$ C using a Malvern Zetasizer Nano ZS (Model #ZEN3600) with a dispersant refractive index of 1.375, viscosity of 0.2860 cP, equilibration time of 10 sec, an attenuator of 7, a count rate of 255.5 kcps, and a polydispersity index of 0.527.

Results and Discussion

All reactions were carried out by injecting colloidal nanoparticles of digenite Cu_{1.8}S into a solution of a Mn²⁺–oleylamine complex in octadecene at various temperatures and allowing the reaction to proceed for 10 minutes before cooling to room temperature. Below 85 °C, there was no evidence of cation exchange, as only digenite Cu_{1.8}S, the starting material, could be isolated. Above 85 °C, MnS products were observed, as shown in Figure 1. This was determined *via* XRD analysis of aliquots taken at various temperatures (up to 100 °C) after a suspension of digenite Cu_{1.8}S nanoparticles in TOP was injected into a Mn²⁺-oleylamine complex in octadecene at 25°C. While the XRD signal intensities are low due to the small sample size of the aliquot, the samples still appear mostly crystalline, with a shift in relative peak intensities between the 65 °C and 85 °C aliquots that is consistent with the transition from digenite Cu_{1.8}S to zincblende MnS in this temperature range.

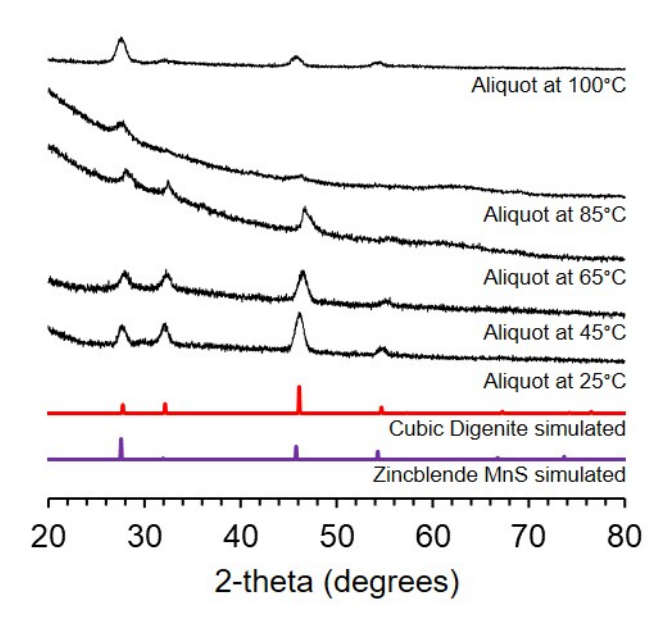


Figure 1. Powder X-ray diffraction (XRD) patterns for aliquots taken at 25 °C, 45 °C, 65 °C, 85 °C, and 100 °C after injecting a TOP-digenite Cu_{1.8}S suspension at 25 °C. Aliquots were taken after holding the reaction solution for 10 min at each temperature. Simulated XRD patterns are shown for reference.^{30,31}

Figure 2a shows an XRD pattern for digenite $Cu_{1.8}S$. The XRD pattern matches well with that of cubic digenite, based on a comparison with a simulated XRD pattern.³¹ A rhombohedral digenite impurity, which is often present in samples of cubic digenite nanoparticles,^{28,32} is structurally related to cubic digenite and transforms to cubic digenite at the temperatures used in the cation exchange reactions.³³

The corresponding TEM image in Figure 2a shows that the digenite nanoparticles are nominally spherical, and the average diameter, based on analysis of 100 particles, is 11.9 ± 1.0 nm. Scherrer analysis of the XRD pattern also indicates an average domain size of 12 nm, suggesting that the particles are single crystalline. Figures 2b, 2c, and 2d show XRD patterns and TEM images for digenite samples reacted with Mn²⁺, as described above, at 100 °C, 200 °C, and 300 °C, respectively. At 100 °C, the dominant product is zincblende MnS, based on comparison with the simulated XRD pattern.³⁰ This is the expected phase, as shown previously, because zincblende MnS has the same ccp sulfur sublattice and tetrahedral cation coordination as the digenite precursor. The average particle diameter by TEM is 10.8 ± 1.4 nm and by XRD is 10 nm, which both are comparable to the digenite precursor. During the reaction at 100 °C, the color changed from black to red-orange, as is typical for this system.^{7,34} At 200 °C, the particles that form have an average diameter of 9.7 ± 2.2 nm, which still is roughly comparable to that of the digenite precursor and the MnS sample formed at 100 °C. The XRD pattern shows that zincblende MnS is the majority phase, but rocksalt MnS is also present as a minority phase. In comparison to the previous system, the color change during this reaction at 200 °C was less significant and resulted in a final product that was much lighter in shade when compared to the color of zincblende MnS at 100 °C. At 300 °C, rocksalt MnS is the only

crystalline phase that is observed, while the particles decrease slightly in average diameter to 8.7 ± 1.5 nm by TEM and 9 nm by XRD. Here, at $300 \, ^{\circ}\text{C}$, a color change following the injection of the digenite precursor appears to transition from yellow to green over a short time-scale. This final green color is consistent with previous reports of rocksalt MnS nanoparticles. The color of the final product of this reaction was distinct from that of the products at lower temperatures, which contained zincblende MnS.

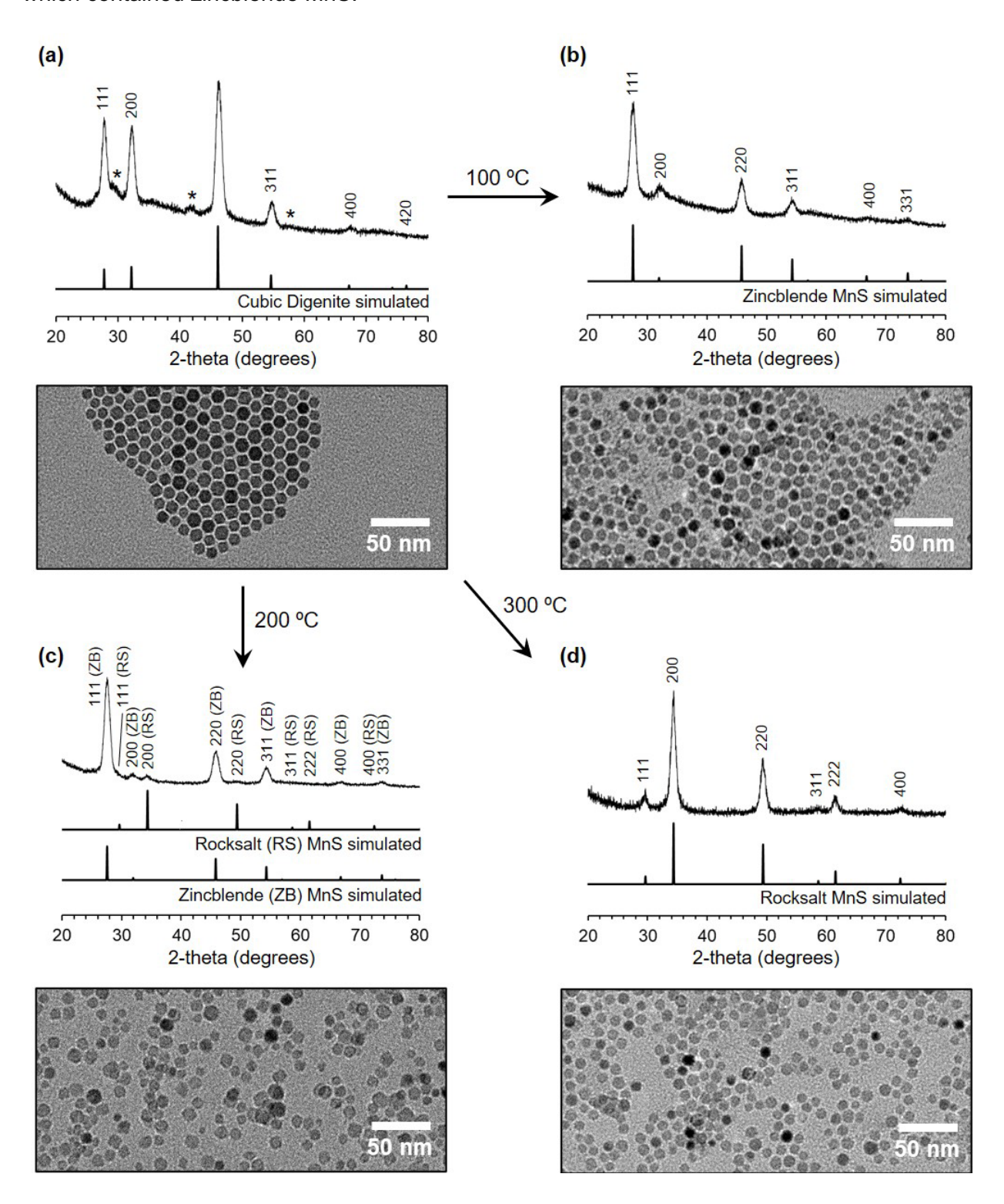


Figure 2. Powder XRD patterns and corresponding TEM images for (a) digenite $Cu_{2-x}S$, (b) the zincblende MnS cation exchange product at 100 °C, (c) the mixture of zincblende MnS and rocksalt MnS products at 200 °C, and (d) the rocksalt MnS product at 300 °C. Simulated XRD patterns are included for reference, ^{30,31} and the reflections corresponding to rhombohedral digenite are indicated with an asterisk (*).

The data in Figure 2 reveal an interesting progression of the reaction. The particle sizes, determined by analysis of the TEM images, are all roughly similar, although with a slight shift toward smaller particle sizes for the samples containing rocksalt MnS. Figure 3 shows these trends in particle size distributions. To summarize, the average particle sizes for digenite $Cu_{1.8}S$, zincblende MnS, and rocksalt MnS were 11.9 ± 1.0 nm, 10.8 ± 1.4 nm, and 8.7 ± 1.5 nm, respectively. Through Scherrer analysis, the average crystalline domain sizes for digenite $Cu_{1.8}S$, zincblende MnS, and rocksalt MnS were 12 nm, 10 nm, and 9 nm, respectively.

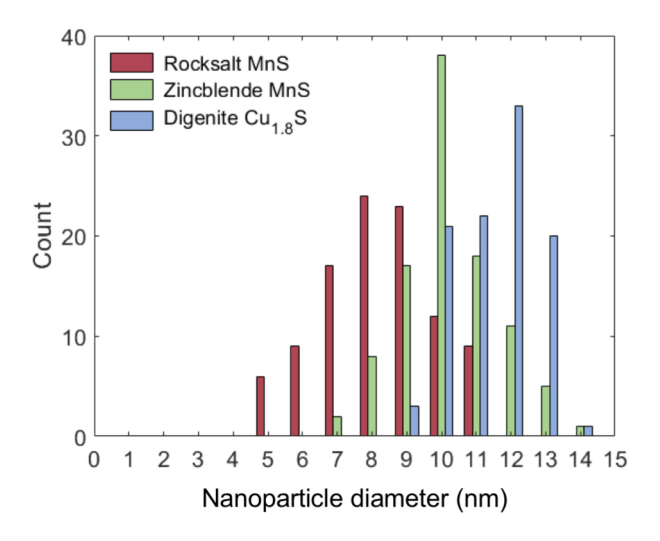


Figure 3. Particle size histograms of digenite $Cu_{1.8}S$ (blue), zincblende MnS (green), and rocksalt MnS (red). The average particle sizes determined by TEM are close to each other, with significant overlap in distributions, although there are noticeable distinctions.

From a crystal structure perspective, the zincblende MnS phase that forms initially upon cation exchange gradually changes to rocksalt MnS as temperature increases. Since zincblende MnS is a metastable phase and rocksalt MnS is the thermodynamically stable phase in the Mn-S binary system, it is not unexpected that the zincblende polymorph transforms to rocksalt at higher temperatures. However, it is important to consider the pathway by which this phase transformation occurred, since the crystallographic relationships between the starting material and the product are sensitive to the reaction pathway. Three possibilities emerge, given the details of the system and reaction. First, it is possible that zincblende MnS formed first upon cation exchange, and then continued heating in solution transformed it to the more stable rocksalt polymorph. Second, it is possible that at the higher cation exchange reaction temperatures, there is sufficient thermal energy for the anion sublattice to rearrange as the cations are shuttling in and out, so that cation exchange and the phase transition happen simultaneously. Third, it is possible that the zincblende and rocksalt polymorphs form through distinct pathways, *i.e.* that zincblende MnS forms through cation exchange and rocksalt MnS

forms by a dissolution/reprecipitation pathway. The data in Figure 2, representing a traditional approach that would be used to address this problem, are unable to differentiate these three plausible scenarios.

We tested whether or not the first scenario – that zincblende MnS formed first upon cation exchange and then transformed, through solution-phase annealing, to rocksalt MnS – was occurring by making zincblende MnS at 100 °C, keeping it in solution, and then heating it to 300 °C. The final product at 300 °C, as well as the product isolated from an aliquot extracted at 150 °C, were both zincblende MnS. The zincblende polymorph therefore persisted to higher temperatures, and we found no evidence for the formation of rocksalt MnS (Figure 4)

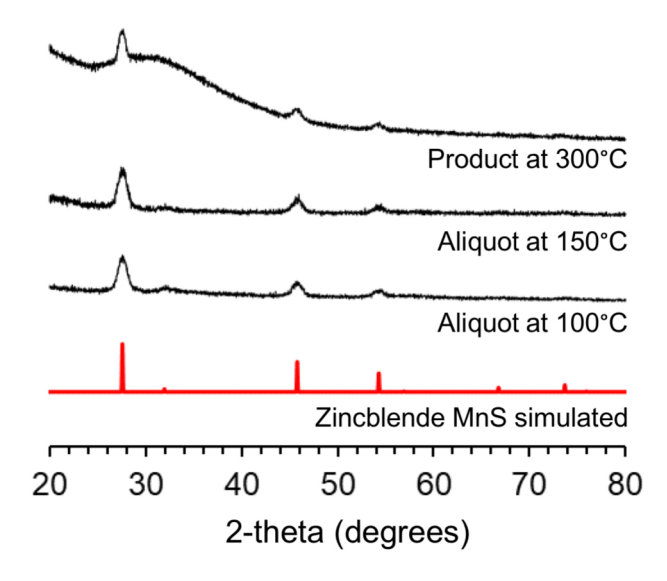
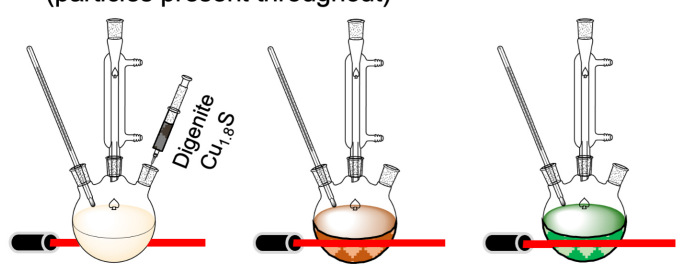


Figure 4. Powder XRD patterns for zincblende MnS formed via cation exchange at 100 °C, an aliquot extracted at 150 °C during solution-phase annealing, and the final product at 300 °C. A simulated XRD pattern for zincblende MnS is included for reference.³⁰

This control experiment rules out the first scenario. We must now differentiate between the second and third scenarios, *i.e.* to determine if cation exchange occurred concomitant with a structural rearrangement or if cation exchange formed zincblende MnS while a dissolution/reprecipitation pathway formed rocksalt MnS. This is where benchtop light scattering allows for insight beyond that which is possible using traditional aliquot methods.

Figure 5 shows a schematic of what is expected to occur when a laser pointer is placed next to the reaction flask for each scenario. For the scenario where the phase transition from zincblende to rocksalt MnS occurs concomitantly with cation exchange, nanoparticles should persist throughout the reaction, and light scattering should appear constant throughout.

a Rocksalt MnS forms via cation exchange (particles present throughout)



b Digenite Cu_{1.8}S dissolves then rocksalt MnS forms (no particles initially)

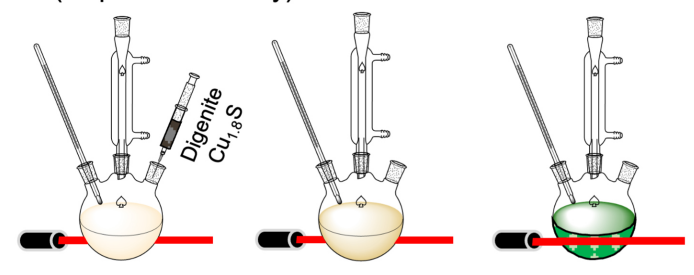


Figure 5. Schematic illustrating how the (a) appearance and persistence or (b) disappearance and then reappearance of light scattering can provide useful insights into the nature of the reaction pathways occurring in solution. In (a), the formation of rocksalt MnS occurs concomitantly with zincblende MnS formation *via* cation exchange (i.e. particles are present during the entire reaction), and in (b), digenite Cu_{1.8}S dissolves and then rocksalt MnS forms separately.

For the scenario where the injected digenite particles dissolve and then rocksalt MnS precipitates in a separate step, initial light scattering from the digenite particles should disappear when the digenite dissolves; scattering should then re-appear once the rocksalt MnS particles form. Figure 6 shows photographs for several control samples performed at room temperature. to correlate the presence and absence of the light scattering with the various possible stages of a reaction. A solution of Mn²⁺-oleylamine complex and octadecene shows no light scattering, while light scattering is observed for that same solution (at room temperature) after injecting digenite nanoparticles. A solution formed by dissolving digenite nanoparticles in trioctylphosphine (TOP) in the presence of air, a known chemical route for etching copper sulfides,^{27,36} shows no light scattering, while light scattering is observed for solutions containing colloidal zincblende and rocksalt MnS nanoparticles. To confirm that light scattering is due to the nanoparticles rather than large aggregates, dynamic light scattering (DLS) was used to evaluate a control sample composed of digenite Cu_{1.8}S nanoparticle dispersed in hexanes. Analysis of the DLS data, shown in Figure S1, revealed a number weighted average of 14.17 nm, which matched well to the average particle diameter determined by TEM (see Figure 2a). This suggests that the observed light scattering from the laser pointer is not due to large aggregates.

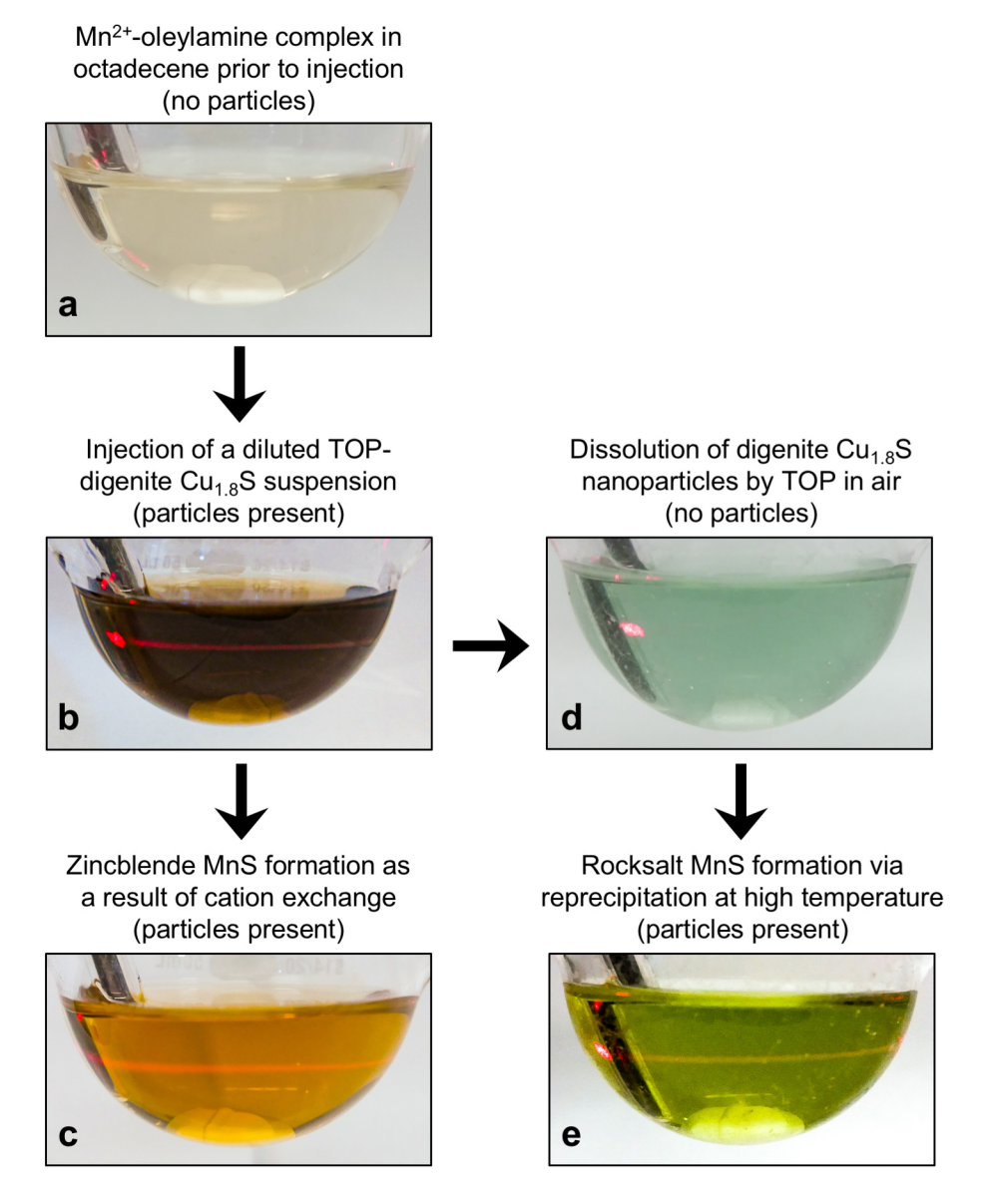


Figure 6. Photographs of control samples taken at room temperature, without stirring, to demonstrate the presence and absence of the light scattering for various possible reaction scenarios. (a) A Mn²⁺-oleylamine complex in octadecene, as would be present prior to injection of the digenite Cu_{1.8}S nanoparticles, does not show the light scattering. (b) After injection of a diluted TOP-digenite Cu_{1.8}S suspension, the light scattering is observed due to the presence of the nanoparticles. (c) Zincblende MnS nanoparticles in solution also exhibit the light scattering; this would be the expected product of Mn²⁺ exchange of digenite Cu_{1.8}S. (d) Digenite Cu_{1.8}S nanoparticles dissolved by TOP in the presence of air do not show the light scattering, because the particles have been consumed. (e) Rocksalt MnS nanoparticles are present, so the light scattering is observed.

Moving from the simulated, idealized scenarios in Figure 6, Figure 7 provides photographs at various time points during the injection of digenite Cu_{1.8}S nanoparticles into a solution of a Mn²⁺–oleylamine complex and octadecene at 100 °C, 200 °C, and 300 °C. Figure 7 also

presents photographs showing that at all three temperatures, the Mn²⁺ metal-ion solutions appeared similar in color and clarity prior to injection of digenite. For each reaction, a red laser pointer was placed next to the reaction flask and photographs were taken immediately upon injection of the digenite Cu_{1.8}S nanoparticles up until 5 min was reached. Figure 7a shows the progression of the reaction at 100 °C, which was shown in Figure 2 to produce zincblende MnS. As expected, immediately upon injection of the digenite nanoparticles, scattering of the red laser pointer light is observed. The scattering of the laser light persists at all time points, indicating that nanoparticles are present throughout the reaction. This is consistent with a cation exchange pathway, which requires nanoparticles to be present at all stages of the reaction.

a 100 °C injection: Nanoparticles appear and persist throughout the reaction (light scattering)

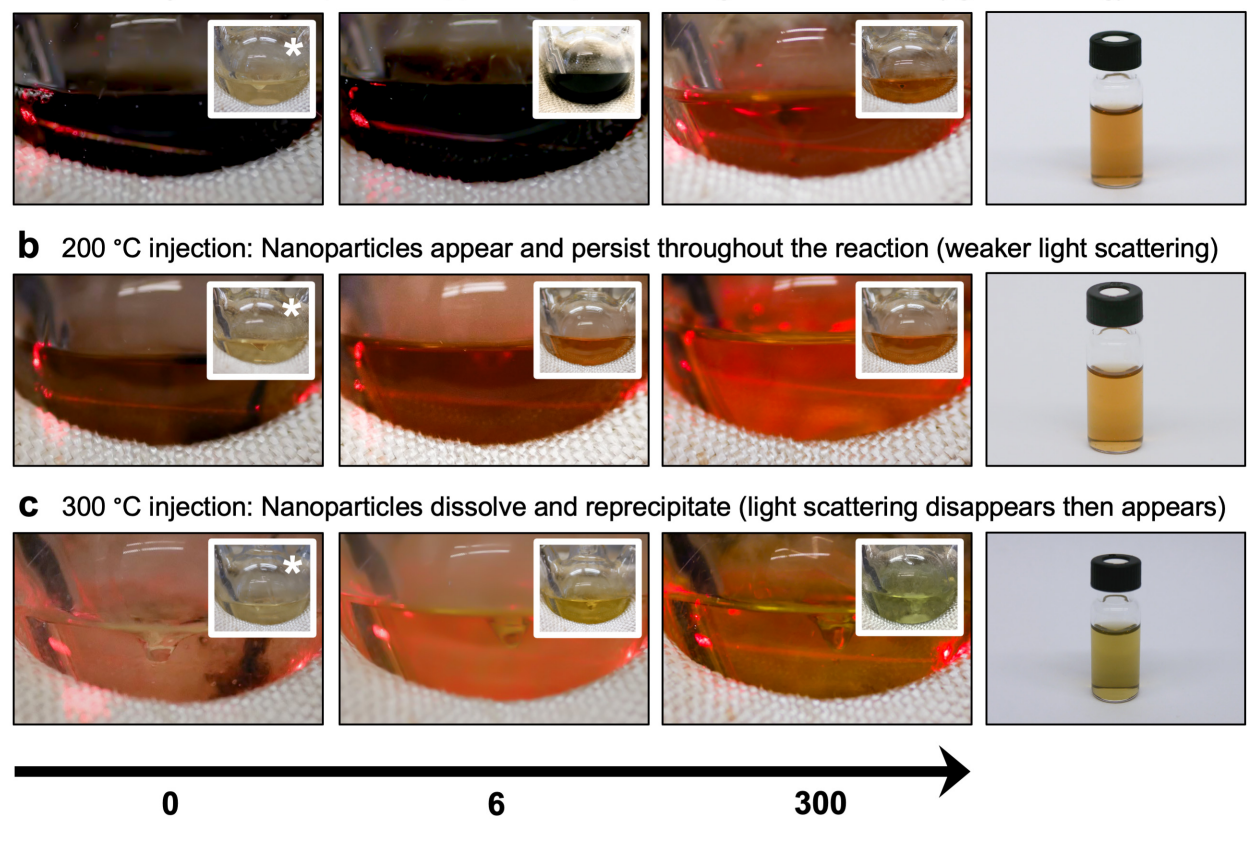


Figure 7. Photographs at various timepoints for three separate reactions where a TOP-digenite Cu_{1.8}S suspension was injected into a Mn²⁺-oleylamine complex in octadecene at (a) 100 °C, (b) 200 °C, and (c) 300 °C. The insets to the images marked with an asterisk (*) indicate that the Mn²⁺ metal-ion solutions all appeared similar in color and clarity prior to the injections. As each of the reactions progressed, either the appearance and persistence, or the disappearance and reappearance, of the light scattering can be observed. The insets to the images without an asterisk correspond to the solutions when the laser pointer was turned off, which can be helpful for observing the color changes (without interference from the laser pointer light) as the reactions progressed. Photographs of the vials containing the products of each sequence are also included to show the progression from red-orange to yellow-orange to green as the product transitioned from zincblende MnS to a mixture of zincblende and rocksalt MnS to just rocksalt MnS.

Time (s)

Data for an identical process at 300 °C is shown in Figure 7c. Analogous to the reaction at 100 °C, light scattering is observed immediately upon injection of the digenite nanoparticles. However, light scattering disappears after a few seconds. This indicates that colloidal nanoparticles are no longer present in significant concentrations in solution. After a short period of time, light scattering re-appears, indicating the presence once again of nanoparticles. Light scattering persists through the final 5-minute time point, where the reaction is confirmed to be complete and the XRD pattern (shown in Figure 2) corresponds to rocksalt MnS.

The laser pointer light scattering data at 300 °C are therefore most consistent with a pathway that does not involve cation exchange, since nanoparticles are not present in significant quantities throughout the entire reaction. Rather, the absence of light scattering at intermediate time points instead suggests a dissolution-reprecipitation pathway, whereby the digenite nanoparticles dissolve and then rocksalt MnS forms directly through a separate precipitation process. Consistent with these observations, at 200 °C where a mixture of zincblende and rocksalt MnS form, light scattering is still observed, but for intermediate times throughout the reaction it appears weaker than at comparable time points in the 100 °C reaction – as expected for a reaction pathway involving a mixture of cation exchange and dissolution/reprecipitation. Also consistent with these observations, the product isolated from a control experiment performed identically to that in Figure 7c but without Mn²⁺ present (i.e. digenite Cu_{1.8}S heated to 300 °C in oleylamine and octadecene) is not digenite Cu_{1.8}S, but rather a mixture of Cu and Cu₂S (Figure S2). Note that the dissolved species would not persist under these conditions at 300 °C, and particles would be expected to form within the time it takes to cool the sample. This result indicates that digenite Cu_{1.8}S is unstable under these conditions and is consistent with the products that would form through a dissolution-reprecipitation pathway, under strongly reducing conditions at 300 °C, in the absence of Mn²⁺.

Conclusions

MnS is an instructive model system for probing reaction pathways because of the accessibility of both metastable and stable phases. When attempts were made at exchanging the Cu^+ cations in digenite $Cu_{1.8}S$ with Mn^{2^+} to form MnS, it was observed that the metastable zincblende polymorph formed at lower temperatures while the thermodynamically preferred rocksalt polymorph formed at higher temperatures. Benchtop light scattering using a laser pointer ruled out higher-temperature pathways that required nanoparticles to be present throughout the reaction. It therefore helped to converge on a dissolution/reprecipitation pathway whereby zincblende MnS formed through cation exchange of digenite $Cu_{1.8}S$ while rocksalt MnS formed through dissolution of the digenite $Cu_{1.8}S$ and subsequent direct formation of MnS nanoparticles.

Benchtop light scattering using a laser pointer provided a useful glimpse into this model reaction that was set up assuming cation exchange is the operable pathway. In this case, it revealed that an alternate dissolution/reprecipitation pathway occurred at higher reaction temperatures, in contrast to cation exchange that occurred at lower temperatures. This is important mechanistically in order to rule out other plausible pathways, such as cation exchange concomitant with a structural rearrangement or initial formation of metastable zincblende MnS followed by transformation to the more stable rocksalt polymorph upon solution-phase annealing. The observation of light scattering is useful and insightful, providing a simple, inexpensive, benchtop probe for uncovering high-level characteristics of a reaction pathway.

Looking beyond the MnS system, this approach has the potential to be broadly useful. As part of optimization studies, it could help to identify upper temperature limits for cation exchange to occur during reactions where competing pathways are possible. It could also help to identify if various reagents cause dissolution and therefore compromise the integrity of an attempted cation exchange reaction. This is especially important, given that several key reagents used in cation exchange reactions, including trialkylphosphines, are known to dissolve copper sulfides. ^{27,28} This approach could also be helpful in studying other cation exchange reactions that are reported to proceed without retention of crystal structure, ^{12–14,37} to help validate cation exchange rather than a dissolution/reprecipitation pathway. More broadly, this approach could shed light on other chemical transformation reactions of nanoparticles that could proceed through a diffusion, exchange, or replacement pathway, which preserves the nanoparticle template, vs. a dissolution/reprecipitation pathway, which does not. Benchtop light scattering therefore provides a characterization tool that is complementary to spectroscopic, diffraction, and microscopy methods, which can be used in the laboratory while a reaction is running.

ASSOCIATED CONTENT

Supporting Information. Dynamic light scattering data and additional X-ray diffraction data. This material is available free of charge *via* the Internet at http://pubs.acs.org.

AUTHOR INFORMATION

Corresponding Author

* R.E. Schaak. Email: res20@psu.edu

Notes

The authors declare no competing financial interest.

ACKNOWLEDGMENT

This work was supported by the U.S. National Science Foundation under grant DMR-1904122. TEM imaging was performed in the Materials Characterization Lab of the Penn State Materials Research Institute. The authors thank Benjamin C. Steimle and Christine D. Keating for helpful discussions

REFERENCES

- (1) Beberwyck, B. J.; Surendranath, Y.; Alivisatos, A. P. Cation Exchange: A Versatile Tool for Nanomaterials Synthesis. *J. Phys. Chem. C* **2013**, *117*, 19759–19770.
- (2) De Trizio, L.; Manna, L. Forging Colloidal Nanostructures via Cation Exchange Reactions. *Chem. Rev.* **2016**, *116*, 10852–10887.
- (3) Jain, P. K.; Amirav, L.; Aloni, S.; Alivisatos, A. P. Nanoheterostructure Cation Exchange: Anionic Framework Conservation. *J. Am. Chem. Soc.* **2010**, *132*, 9997–9999.
- (4) Hee Son, D.; Hughes, S. M.; Yin, Y.; Alivisatos, A. P. Cation Exchange Reactions in Ionic Nanocrystals. *Science* **2004**, *306*, 1009–1012.
- (5) Li, H.; Zanella, M.; Genovese, A.; Povia, M.; Falqui, A.; Giannini, C.; Manna, L.

- Sequential Cation Exchange in Nanocrystals: Preservation of Crystal Phase and Formation of Metastable Phases. *Nano Lett.* **2011**, *11*, 4964–4970.
- (6) Powell, A. E.; Hodges, J. M.; Schaak, R. E. Preserving Both Anion and Cation Sublattice Features during a Nanocrystal Cation-Exchange Reaction: Synthesis of Metastable Wurtzite-Type CoS and MnS. *J. Am. Chem. Soc.* **2016**, *138*, 471–474.
- (7) Fenton, J. L.; Schaak, R. E. Structure-Selective Cation Exchange in the Synthesis of Zincblende MnS and CoS Nanocrystals. *Angew. Chem., Int. Ed.* **2017**, *56*, 6464–6467.
- (8) Fenton, J. L.; Steimle, B. C.; Schaak, R. E. Structure-Selective Synthesis of Wurtzite and Zincblende ZnS, CdS, and CulnS₂ Using Nanoparticle Cation Exchange Reactions. *Inorg. Chem.* **2019**, *58*, 672–678.
- (9) Schaak, R. E.; Steimle, B. C.; Fenton, J. L. Made-to-Order Heterostructured Nanoparticle Libraries. *Acc. Chem. Res.* **2020**, *53*, 2558–2568.
- (10) Kan, S.; Felner, I.; Banin, U. Synthesis, Characterization, and Magnetic Properties of α-MnS Nanocrystals. *Isr. J. Chem.* **2001**, *41*, 55–61.
- (11) Yang, X.; Wang, Y.; Sui, Y.; Huang, X.; Cui, T.; Wang, C.; Liu, B.; Zou, G.; Zou, B. Size-Controlled Synthesis of Bifunctional Magnetic and Ultraviolet Optical Rock-Salt Mns Nanocube Superlattices. *Langmuir* **2012**, *28*, 17811–17816.
- (12) Wark, S. E.; Hsia, C. H.; Dong, H. S. Effects of Ion Solvation and Volume Change of Reaction on the Equilibrium and Morphology in Cation-Exchange Reaction of Nanocrystals. J. Am. Chem. Soc. 2008, 130, 9550–9555.
- (13) Jeong, S.; Han, J. H.; Jang, J. T.; Seo, J. W.; Kim, J. G.; Cheon, J. Transformative Two-Dimensional Layered Nanocrystals. *J. Am. Chem. Soc.* **2011**, *133*, 14500–14503.
- (14) Ramirez, O.; Ramasamy, P.; Chan Choi, Y.; Lee, J. S. Morphology Transformation of Chalcogenide Nanoparticles Triggered by Cation Exchange Reactions. *Chem. Mater.* **2019**, *31*, 268–276.
- (15) Bøjesen, E. D.; Jensen, K. M. Ø.; Tyrsted, C.; Lock, N.; Christensen, M.; Iversen, B. B. In Situ Powder Diffraction Study of the Hydrothermal Synthesis of ZnO Nanoparticles. *Cryst. Growth Des.* **2014**, *14*, 2803–2810.
- (16) Staniuk, M.; Hirsch, O.; Kränzlin, N.; Böhlen, R.; Van Beek, W.; Abdala, P. M.; Koziej, D. Puzzling Mechanism behind a Simple Synthesis of Cobalt and Cobalt Oxide Nanoparticles: In Situ Synchrotron X-Ray Absorption and Diffraction Studies. *Chem. Mater.* 2014, 26, 2086–2094.
- (17) Polte, J.; Ahner, T. T.; Delissen, F.; Sokolov, S.; Emmerling, F.; Thünemann, A. F.; Kraehnert, R. Mechanism of Gold Nanoparticle Formation in the Classical Citrate Synthesis Method Derived from Coupled in Situ XANES and SAXS Evaluation. *J. Am. Chem. Soc.* **2010**, *132*, 1296–1301.
- (18) Liang, W. I.; Zhang, X.; Zan, Y.; Pan, M.; Czarnik, C.; Bustillo, K.; Xu, J.; Chu, Y. H.; Zheng, H. In Situ Study of Fe₃Pt–Fe₂O₃ Core-Shell Nanoparticle Formation. *J. Am. Chem. Soc.* **2015**, *137*, 14850–14853.
- (19) Jungjohann, K. L.; Bliznakov, S.; Sutter, P. W.; Stach, E. A.; Sutter, E. A. In Situ Liquid Cell Electron Microscopy of the Solution Growth of Au-Pd Core-Shell Nanostructures. *Nano Lett.* **2013**, *13*, 2964–2970.
- (20) Steimle, B. C.; Fagan, A. M.; Butterfield, A. G.; Lord, R. W.; McCormick, C. R.; Di Domizio, G. A.; Schaak, R. E. Experimental Insights into Partial Cation Exchange Reactions for Synthesizing Heterostructured Metal Sulfide Nanocrystals. *Chem. Mater.* **2020**, *32*, 5461–5482.
- (21) Dorn, A.; Allen, P. M.; Harris, D. K.; Bawendi, M. G. In Situ Electrical Monitoring of Cation Exchange in Nanowires. *Nano Lett.* **2010**, *10*, 3948–3951.
- (22) Moser, A.; Yarema, M.; Lin, W. M. M.; Yarema, O.; Yazdani, N.; Wood, V. In Situ Monitoring of Cation-Exchange Reaction Shell Growth on Nanocrystals. *J. Phys. Chem. C* **2017**, *121*, 24345–24351.

- (23) Miszta, K.; Dorfs, D.; Genovese, A.; Kim, M. R.; Manna, L. Cation Exchange Reactions in Colloidal Branched Nanocrystals. *ACS Nano* **2011**, *5*, 7176–7183.
- (24) Smith, J. G.; Yang, Q.; Jain, P. K. Identification of a Critical Intermediate in Galvanic Exchange Reactions by Single-Nanoparticle-Resolved Kinetics. *Angew. Chem., Int. Ed.* **2014**, *53*, 2867–2872.
- (25) Tyndall, J. On the Blue Color of the Sky, the Polarization of Skylight, and Polarization of Light by Cloudy Matter Generally. *J. Franklin Inst.* **1869**, 34–40.
- (26) Kraemer, E. O.; Dexter, S. T. The Light-Scattering Capacity (Tyndall Effect) and Colloidal Behavior of Gelatine Sols and Gels. *J. Phys. Chem.* **1927**, 764–782.
- (27) Nelson, A.; Ha, D. H.; Robinson, R. D. Selective Etching of Copper Sulfide Nanoparticles and Heterostructures through Sulfur Abstraction: Phase Transformations and Optical Properties. *Chem. Mater.* **2016**, *28*, 8530–8541.
- (28) Liu, L.; Zhong, H.; Bai, Z.; Zhang, T.; Fu, W.; Shi, L.; Xie, H.; Deng, L.; Zou, B. Controllable Transformation from Rhombohedral Cu_{1.8}S Nanocrystals to Hexagonal CuS Clusters: Phase- and Composition-Dependent Plasmonic Properties. *Chem. Mater.* **2013**, 25, 4828–4834.
- (29) Zhou, D.; Liu, D.; Xu, W.; Yin, Z.; Chen, X.; Zhou, P.; Cui, S.; Chen, Z.; Song, H. Observation of Considerable Upconversion Enhancement Induced by Cu_{2-x}S Plasmon Nanoparticles. *ACS Nano* **2016**, *10*, 5169–5179.
- (30) Villars, P. Pearson's Handbook of Crystallographic Data for Intermetallic Phases.; 1998.
- (31) Will, G.; Hinze, E.; Abdelrahman, A. R. M. Crystal Structure Analysis and Refinement of Digenite, Cu_{1.8}S, in the Temperature Range 20 to 500 C under Controlled Sulfur Partial Pressure. *Eur. J. Mineral.* **2002**, *14*, 591–598.
- (32) Coughlan, C.; Ibáñez, M.; Dobrozhan, O.; Singh, A.; Cabot, A.; Ryan, K. M. Compound Copper Chalcogenide Nanocrystals. *Chem. Rev.* **2017**, *117*, 5865–6109.
- (33) Steimle, B. C.; Lord, R. W.; Schaak, R. E. Phosphine-Induced Phase Transition in Copper Sulfide Nanoparticles Prior to Initiation of a Cation Exchange Reaction. *J. Am. Chem. Soc.* **2020**, *142*, 13345–13349.
- (34) Yang, X.; Wang, Y.; Wang, K.; Sui, Y.; Zhang, M.; Li, B.; Ma, Y.; Liu, B.; Zou, G.; Zou, B. Polymorphism and Formation Mechanism of Nanobipods in Manganese Sulfide Nanocrystals Induced by Temperature or Pressure. *J. Phys. Chem. C* **2012**, *116*, 3292–3297.
- (35) Moloto, N.; Moloto, M. J.; Kalenga, M.; Govindraju, S.; Airo, M. Synthesis and Characterization of MnS and MnSe Nanoparticles: Morphology, Optical and Magnetic Properties. *Opt. Mater. (Amst).* **2014**, *36*, 31–35.
- (36) Butterfield, A. G.; Steimle, B. C.; Schaak, R. E. Retrosynthetic Design of Morphologically Complex Metal Sulfide Nanoparticles Using Sequential Partial Cation Exchange and Chemical Etching. *ACS Mater. Lett.* **2020**, *2*, 1106–1114.
- (37) Mu, L.; Wang, F.; Sadtler, B.; Loomis, R. A.; Buhro, W. E. Influence of the Nanoscale Kirkendall Effect on the Morphology of Copper Indium Disulfide Nanoplatelets Synthesized by Ion Exchange. *ACS Nano* **2015**, *9*, 7419–7428.

Table of Contents Graphic

